High Power Laser Science and Engineering, (2019), Vol. 7, e17, 8 pages.

doi:10.1017/hpl.2019.3

Maser radiation from collisionless shocks: application to astrophysical jets

D. C. Speirs[1], K. Ronald[1], A. D. R. Phelps[1], M. E. Koepke[2], R. A. Cairns[3], A. Rigby[4], F. Cruz[5], R. M. G. M. Trines[6], R. Bamford[6], B. J. Kellett[6], B. Albertazzi[7], J. E. Cross[8], F. Fraschetti[9], P. Graham[10], P. M. Kozlowski[8], Y. Kuramitsu[11], F. Miniati[8], T. Morita[12], M. Oliver[8], B. Reville[13], Y. Sakawa[12], S. Sarkar[8], C. Spindloe[6], M. Koenig[7], L. O. Silva[5], D. Q. Lamb[14], P. Tzeferacos[8,14], S. Lebedev[15], G. Gregori[8,14], and R. Bingham[1,6]

[1]*Department of Physics, SUPA, University of Strathclyde, Glasgow, G4 0NG, UK*

[2]*Department of Physics, West Virginia University, Morgantown, WV 26506-6315, USA*

[3]*School of Mathematics and Statistics, University of St. Andrews, Fife, KY16 9SS, UK*

[4]*Department of Physics, University of Oxford, Parks Road, Oxford, OX1 3PU, UK*

[5]*GoLP/Instituto de Plasmas e Fusão Nuclear, Instituto Superior Técnico, Universidade de Lisboa, 1049-001 Lisbon, Portugal*

[6]*STFC Rutherford Appleton Laboratory, Chilton, Didcot, Oxon, OX11 0QX, UK*

[7]*Laboratoire pour l'Utilisation de Lasers Intenses, UMR7605, CNRS CEA, Université Paris VI Ecole Polytechnique, 91128 Palaiseau Cedex, France*

[8]*Department of Physics, University of Oxford, Parks Road, Oxford, OX1 3PU, UK*

[9]*Departments of Planetary Sciences and Astronomy, University of Arizona, Tucson, AZ 85721, USA*

[10]*AWE, Aldermaston, Reading, West Berkshire, RG7 4PR, UK*

[11]*Department of Physics, National Central University, Taoyuan 320, Taiwan*

[12]*Institute of Laser Engineering, Osaka University, 2-6 Yamadaoka, Suita, Osaka 565-0871, Japan*

[13]*School of Mathematics and Physics, Queen's University Belfast, Belfast, BT7 1NN, UK*

[14]*Department of Astronomy and Astrophysics, University of Chicago, Chicago, IL 60637, USA*

[15]*Imperial College London, London, SW72AZ, UK*

(Received 30 August 2018; revised 9 January 2019; accepted 21 January 2019)

Abstract

This paper describes a model of electron energization and cyclotron-maser emission applicable to astrophysical magnetized collisionless shocks. It is motivated by the work of Begelman, Ergun and Rees [Astrophys. J. **625**, 51 (2005)] who argued that the cyclotron-maser instability occurs in localized magnetized collisionless shocks such as those expected in blazar jets. We report on recent research carried out to investigate electron acceleration at collisionless shocks and maser radiation associated with the accelerated electrons. We describe how electrons accelerated by lower-hybrid waves at collisionless shocks generate cyclotron-maser radiation when the accelerated electrons move into regions of stronger magnetic fields. The electrons are accelerated along the magnetic field and magnetically compressed leading to the formation of an electron velocity distribution having a horseshoe shape due to conservation of the electron magnetic moment. Under certain conditions the horseshoe electron velocity distribution function is unstable to the cyclotron-maser instability [Bingham and Cairns, Phys. Plasmas **7**, 3089 (2000); Melrose, Rev. Mod. Plasma Phys. **1**, 5 (2017)].

Keywords: laboratory astrophysics; plasma physics; particle acceleration; plasma-wave instabilities

Correspondence to: D. C. Speirs, Department of Physics, University of Strathclyde, John Anderson Building, Glasgow, G4 0NG, UK. Email: david.c.speirs@strath.ac.uk

1. Introduction

Blazar jets are beam-like linear features observable over a broad range of frequencies and generated perpendicularly to the accretion disc of super massive black holes[1, 2]. They normally extend over intergalactic distances (many thousands of light years) and are observed to generate highly non-thermal radio emission at frequencies ranging from a few to 100s of GHz, with intrinsic brightness temperatures in excess of 10^{14} K[3]. Begelman *et al.* suggested[3] that a cyclotron-maser instability is responsible for the generation of these emissions in the low density ($\omega_{ce} > \omega_{pe}$), magnetized plasma of the jet[3–5], where ω_{ce} and ω_{pe} are the electron-cyclotron and plasma frequencies, respectively. It is assumed that within the jet, small scale magnetic mirrors/convergent flux tubes may be formed via shocks or hydrodynamic instabilities, providing the environment for generating the required electron velocity distribution[3, 4].

The background magnetic field within a blazar jet is assumed to be very high[6] leading to large electron cyclotron frequencies for the energetic electron population within the jet in the 1–100 GHz range. This results in $\omega_{ce} \gg \omega_{pe}$[3], a necessary condition for the cyclotron-maser instability. Begelman, Ergun and Rees[3] deduced values for the ratio of cyclotron frequency to plasma frequency that indicate the efficiency of the maser-emission process for blazar jets could be an order of magnitude greater than for the auroral maser-emission process. Gurnett estimated the conversion efficiency from electron beam to electromagnetic (EM) radiation to be about 1% in the auroral zone[7]. Begelmann, Ergun and Rees[3] concluded that the radiation could indeed be due to the cyclotron-maser instability driven by an electron horseshoe/ring distribution. In previous work it has been shown that a suitable ring-type velocity distribution may be generated directly via the surfatron mechanism, through energization of particles perpendicular to the magnetostatic field[8]. We have also proposed an alternative scheme by which electrons may be accelerated and magnetically compressed within a magnetised collisionless shock, resulting in a suitable horseshoe or crescent-type velocity distribution[4]. Both mechanisms are viable within the turbulent, highly magnetised plasma of a blazar jet, with field-aligned currents and small scale magnetic mirrors expected to be observed in association with quasi-perpendicular collisionless shocks[3]. Counter-streaming ion populations formed at such shocks can excite lower hybrid waves via the modified two-stream instability[9, 10]. These waves are capable of accelerating electrons parallel to the magnetic field and up to high energies[11–13]. The resultant energetic electron tail distributions can then experience magnetic compression when moving from the upstream to downstream region of the magnetised collisionless shock, producing a horseshoe or crescent-type distribution function which is unstable to the cyclotron-maser instability. This model[14] has been used to account for acceleration of energetic particles at comets[15] and within supernova remnants[16, 17]. The same model has also been applied successfully to explain energetic particles in artificial releases from spacecraft[18] and the physics of collisionless shocks near lunar magnetic abnormalities[19, 20] and in the globally induced lunar magnetosphere[21]. Recently, this model has been tested in a laser-plasma experiment[22] and successfully modelled by using PIC (particle-in-cell) codes[23]. The escape of cyclotron-maser radiation from a blazar jet has been previously considered in some detail[3, 5], with various factors debated including second harmonic cyclotron absorption and synchrotron absorption. Both mechanisms are potentially the most significant impediments, but can be suitably accounted for[3] in the case of a blazar jet. Within the turbulent magnetised plasma of a jet, the second harmonic absorption layer is considered to occur perpendicularly to the magnetostatic field[3], with the generated X-mode radiation also propagating radially outwards, almost perpendicularly to the magnetic field. It was shown by Begelman *et al.* that the thickness of the second harmonic layer can be approximated as $\sim r_m \omega_{pe}/\omega_{ce}$ which is relatively thin and results in attenuation of 10%, where r_m is the radius of the jet at the emission region. Another consideration is the potential for refraction of the generated radiation due to the gradient in plasma density associated with the quasi-perpendicular shock. From our previous consideration for the terrestrial auroral case[24], this could result in R-mode like radiation propagating parallel to the magnetostatic field and an associated reduction in cyclotron-wave coupling efficiency for second harmonic absorption at the associated magnetic field resonance. Laboratory astrophysics is an exciting area pioneered by several groups[22, 25–29]. The scaling relationships that allow laboratory experiments to investigate astrophysical phenomena are well established and routinely used to devise laboratory parameter regimes that have astrophysical relevance[30]. Laboratory experiments conducted by Lebedev *et al.*[28] for the study of high speed plasma jets can in particular be comparatively considered with reference to astrophysical regimes via Ryutov's scaling[30]. In the current context, the experiments that are described and reviewed in this article compare well with the astrophysical scenario under consideration. From this point, the paper is organised as follows. Section 2: we describe electron acceleration by lower hybrid waves at collisionless shocks. Section 3: we describe the cyclotron-maser emission model. Section 4: we summarise and review our findings and implications of the results.

2. Electron acceleration and cyclotron-maser emission

2.1. Electron acceleration by lower-hybrid waves

Lower-hybrid waves have been used in the laboratory for some time particularly with regard to generating high energy electron tails for current drive in tokamaks[31]. They have also been associated with a number of space and astrophysics particle acceleration problems in particular collisionless shock acceleration in flares[11], bow shocks in magnetospheres[32], supernova remnants[17], jets[4] and galaxy clusters. Although they have been inferred in satellite data from these systems for many years, laboratory experiments provide a controlled environment allowing reproducible results supporting space observations and validating data from simulation codes[23]. The resonant interaction between lower-hybrid turbulence and electrons can result in field-aligned electron acceleration[12, 13, 33–35]. These waves are most probably excited by the modified two-stream instability[10] resulting from the interaction between a collisionless shock and the ion species in the ambient plasma. In this interaction a pressure wave or shock wave forms resulting in the perturbation of ion trajectories and collective gyration due to acceleration with respect to the ambient magnetic field. These ions under the action of $\underline{E} \times \underline{B}$ evolve a monoenergetic ion ring distribution in the plasma. This distribution of ions drives the modified two-stream instability described by the following dispersion relation[32, 33]

$$\frac{\omega_{lh}^2}{\Omega^2} + \frac{\omega_{ce}^2}{\Omega^2}\frac{k_\parallel^2}{k^2+\omega_{pe}^2/c^2} + 8\pi^2 i \int \mathrm{d}v_\parallel \int_{\Omega/k_\perp}^{\infty} \mathrm{d}v_\perp \frac{\partial f_p/\partial v_\perp}{\sqrt{k_\perp^2 v_\perp^2 - \Omega^2}} = 1 + \frac{\omega_{pe}^2}{k^2 c^2}, \tag{1}$$

where $f_p(v_\perp, v_\parallel)$ is the distribution function of the reflected protons in terms of the perpendicular velocity $v_\perp$ and axial velocity $v_\parallel$, ω_{lh} is the lower-hybrid frequency, $k_\parallel$ and $k_\perp$ are the axial and perpendicular wavenumbers, respectively, and k is the wavenumber. We assumed that as a result of ion gyration in the ambient magnetic field, particles are completely mixed over phase of rotation and establish a gyrotropic distribution $f(v_\perp, v_\parallel)$, contrary to the case of a nongyrotropic plane beam distribution. The instability excites lower-hybrid waves having the following dispersion law[33]

$$\Omega^2 = \frac{\omega_{lh}^2\left(1+\frac{\beta}{2k^2\rho^2}\right) + \omega_{ce}^2\frac{k_\parallel^2}{k^2}}{(1+\beta/2k^2\rho^2)^2}, \tag{2}$$

where $\beta = 8\pi n_0 T_e/B_0^2$ is the ratio of the plasma kinetic pressure to the magnetic pressure, $\rho = \sqrt{T_e/m_e}/\omega_{ce}$ is the electron gyroradius calculated with the electron temperature T_e, m_e is the electron mass, B_0 is the magnetic flux density and n_0 is the plasma density.

The integral over $v_\perp$ on the l.h.s. of Equation (1) can be easily calculated giving the following expression for the growth rate[32], where n_{rp} is the reflected proton density and m_p is the proton mass.

$$\gamma_{gr} = \frac{1}{2}\frac{n_{rp}}{n_0}\frac{\Omega^2\omega_{lh}^2}{k^3 v_\perp^3}\frac{1}{1+\frac{\beta}{2k^2\rho^2}}. \tag{3}$$

In order for the instability to be viable it needs to develop on a distance scale of $r \approx 10u/\gamma_{gr}$ which must also be shorter than the physical dimensions of the interaction region, where u is the shock velocity (of order 3×10^7 m·s^{-1} in the case of the blazar jet). The corresponding distance scale r for generating the lower-hybrid turbulence would therefore be ∼30 km in the blazar jet environment.

The wave spectrum is centred on the average energy ε_e, which can be obtained from energy balance between the ambient ions species and the accelerated electrons $\alpha n_{rp} m_p u^3 \approx n_e \varepsilon_e (\varepsilon_e/m_e)^{1/2}$, where α is the transformation efficiency from reflected protons to electrons which we take as 0.1%, their density n_e can be estimated by balancing the growth rate of the instability initiated by ambient protons γ_p with Landau damping due to electrons γ_e moving parallel to the magnetic field,

$$\gamma_p + \gamma_e \sim \frac{\partial f_p}{\partial v} + \frac{m_p}{m_e}\frac{\partial f_e}{\partial v_\parallel} \approx 0. \tag{4}$$

Equation (4) can be rewritten as

$$\frac{n_e}{\varepsilon_e} \approx \frac{n_{rp}}{m_p u^2} \tag{5}$$

and together with the above equation for the energy balance gives an estimate for the accelerated electron energy $\varepsilon_e \approx \alpha^{2/5}(m_e/m_p)^{1/5} m_p u^2$ and their number density $n_e \approx n_{rp}\alpha^{2/5}(m_e/m_i)^{1/5}$[14, 15]. This corresponds to electron energies of 450 keV and a number density n_e of 5% of the reflected proton density n_{rp}.

Recent PIC simulations conducted by using OSIRIS[23] predicted electron acceleration via lower-hybrid turbulence of $\varepsilon_e^{\mathrm{PIC}} \sim 75$ keV while an associated scaled laboratory experiment[22] (with differing electron-ion mass ratio and ion velocity u) demonstrated electron energization to $\varepsilon_e^{\mathrm{LAB}} \sim$ 45 eV. This new laboratory experiment[22] confirmed that the analytical estimates for the average energy ϵ_e and number density n_e of accelerated electrons (described by the equations above) are in good agreement with the experimental results, as were the numerical simulations[23]. This

strengthens the theoretical model describing lower-hybrid electron acceleration at collisionless shocks predicted by a number of authors. In Ref. [3], it is argued that electrons accelerated at collisionless shocks have the possibility of being magnetically compressed giving rise to horseshoe-type electron velocity distribution functions which are unstable to the generation of maser radiation[3–5, 36]. Some of the present authors have conducted extensive laboratory experiments to study maser radiation from electron horseshoe/ring distributions[37–39]. They adopted an electron energy (~50–100 keV) and magnetic flux density (~0.5 T) similar to those associated with the blazar jet parameters[3]. The experimental details of maser radiation from accelerated electrons are reported in Section 3.

2.2. Electron cyclotron-maser instability

In this section we consider the stability of a horseshoe shaped electron velocity distribution with respect to a cyclotron-maser instability resulting in R-X mode waves propagating perpendicularly to a magnetostatic field[36, 40]. To obtain the horseshoe distribution function, we consider a drifting Maxwellian having a drift velocity well above the thermal speed. This is typical for electrons accelerated by lower-hybrid turbulence. The particle population then moves into an increasing magnetic field where the distribution function is readily calculated by conservation of total energy and magnetic moment. We use the resulting distribution function in the dispersion relation for the R-X mode, obtainable from the susceptibility tensor given by Ref. [41], assuming that the frequency is close to the electron-cyclotron frequency and that the Larmor radius for typical electron velocities is much less than the wavelength of the wave. We need only consider the susceptibility to lowest order in $k_\perp v_\perp/\omega_{ce}$ as a result of this latter condition. Neglecting all but the zero-order terms, we get the cold plasma result[41]. To a first approximation, it is only necessary to account for the velocity distribution of the electrons in the resonant integral involving $1/(\omega - \omega_{ce})$, where ω_{ce} is the relativistic electron-cyclotron frequency $eB/\gamma m_e$, with e the electron charge, B the magnetic field, γ the Lorentz factor, and m_e the electron rest mass. We must account for the relativistic shift of the cyclotron frequency in the resonant term, as this picks out a particular group of resonant electrons and results in either damping or growth of the wave. In terms of momentum p we have

$$\omega_{ce} = \omega_{e0}\left(1 + \frac{p^2}{m_e^2 c^2}\right)^{-1/2}, \tag{6}$$

where ω_{e0} is the non-relativistic electron-cyclotron frequency. We can simply take the cold plasma result for the real part of the resonant integral. Although this is proportional to $1/(\omega - \omega_{e0})$ and appears to be near-singular at the resonance, the $1/(\omega - \omega_{e0})$ factors in the real part of the dispersion relation cancel out, resulting in smooth behaviour in the vicinity of the cyclotron frequency. Small corrections to the cyclotron frequency are not necessary in the real part of the dispersion relation. The refractive index N for the R-X mode, which propagates perpendicularly to the magnetostatic field, is well known and given by Ref. [41],

$$N^2 = (\epsilon_\perp^2 - \epsilon_{xy}^2)/\epsilon_\perp, \tag{7}$$

with the dielectric tensor elements given by

$$\epsilon_\perp = 1 - \frac{1}{2}\frac{\omega_p^2}{\omega(\omega + \omega_{e0})} + A, \tag{8}$$

$$\epsilon_{xy} = \frac{1}{2}\frac{\omega_{pe}^2}{\omega(\omega + \omega_{e0})} + A, \tag{9}$$

and

$$A = \frac{1}{4}\frac{\omega_{pe}^2}{\omega}\int_0^\infty 2\pi\, p_\perp \,\mathrm{d}p_\perp \times \int_{-\infty}^{\infty} \mathrm{d}p_\parallel \frac{1}{\omega - \omega_{ce}} p_\perp \frac{\partial f_e}{\partial p_\perp}. \tag{10}$$

In order to obtain this we have only included the 1st terms in the sum over harmonics, and used the small argument expansion $J_1(x) \approx x/2$, where $x = k_\perp v_\perp/\omega_{ce}$. If we switch to spherical polar coordinates (p, μ, ϕ), and substitute the usual angle θ with $\mu = \cos\theta = p_\parallel/p$ we then get

$$A = -\frac{1}{2}\frac{\omega_{pe}^2}{\omega(\omega - \omega_{e0})} - \frac{i}{2}\frac{\omega_{pe}^2}{\omega_{e0}}\int_1^{-1}(1-\mu^2)p_0^2\gamma_0^2 \times \left(\frac{\partial f_e}{\partial p} - \frac{\mu}{p_0}\frac{\partial f_e}{\partial \mu}\right)_{|p=p_0|} \mathrm{d}\mu, \tag{11}$$

where $\gamma = (1 + p^2)^{1/2}$ and p_0 is the resonant momentum, $p_0 = m_e c[2(\omega_{e0} - \omega)/\omega_{ce}]^{1/2}$. A complete analysis of the dispersion relation for waves propagating perpendicularly to the magnetostatic field can be found in Ref. [41].

From Equations (8), (9) and (10) we can examine the stability of Equation (7) with respect to induced emission of right hand polarized radiation.

We consider the initial beam to be a drifting Maxwellian moving into a strong magnetic field region. Figure 1 illustrates the characteristic horseshoe or crescent distribution generated when the beam moves into a stronger field region. Using the distribution shown in Figure 1, we obtain the spatial growth rate shown in Figure 2 for two different beam energies. The imaginary part of the refractive index is plotted as a function of frequency for mean beam energies of 100 keV and 500 keV, both with a 1% energy spread and a magnetic field ratio of 20. Unstable wave growth occurs for (and in proportion to) negative values for the imaginary part of the refractive index. With reference to

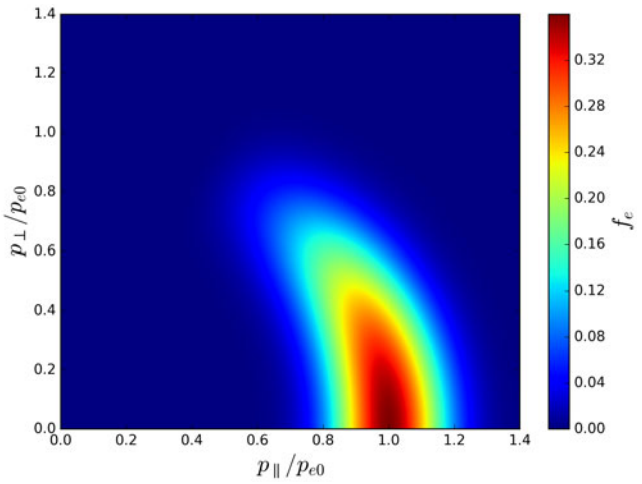

Figure 1. Perpendicular and parallel components of electron momentum (normalized to the mean electron momentum p_{e0}) for an evolved horseshoe distribution function, with the contours representing constant phase-space density.

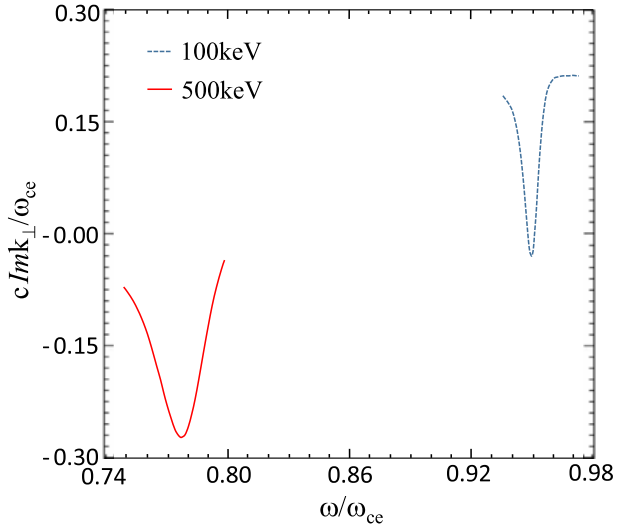

Figure 2. Imaginary part of the refractive index as a function of frequency for a mean beam energy of 100 keV and a thermal spread of 1 keV, and a mean beam energy of 500 keV and a thermal spread of 5 keV. The magnetic field ratio is taken to be 20.

Figure 2, the maximum growth rate for the 500 keV beam is therefore more than 5 times greater than for the 100 keV beam, with a growth spectral bandwidth that is around 10 times larger. The analysis presented above considers strictly perpendicular propagation. We also calculated the growth rates for modes that contain a parallel wavenumber component, finding that modes that propagate more than about 50° to the perpendicular direction do not grow. We find that the fastest growing component is for propagation purely perpendicular to the magnetostatic field. The region of instability in frequency space is extremely narrow with a bandwidth $\delta\omega/\omega$ on the order of 0.5%.

It should be noted that the wave emission due to a horseshoe or ring distribution is primarily in the plane perpendicular to the magnetic field, spectrally close to the electron-cyclotron frequency. For higher electron energies the frequency decreases due to the relativistic mass increase, clearly evident when comparing the maximum growth rates shown in Figure 2. A parallel component of wavenumber incorporates a Doppler shift into the resonance condition, resulting in the resonant particles no longer lying on a sphere in momentum space, centred on the origin. The implications are that for any significant Doppler shift, resonant particles will no longer lie in the portion of the electron velocity distribution for which there is a positive slope. The growth rate therefore falls off as we move away from perpendicular propagation, with the peak wave emission expected in the plane perpendicular to the magnetostatic field. As expected the instability is sensitive to the ratio of the electron-cyclotron frequency to the plasma frequency ω_{ce}/ω_{pe}. For $\omega_{ce} \gg \omega_{pe}$ we expect strong growth occurring in a low background plasma density, where beam instabilities are not strong enough to disrupt the electron velocity and spatial distribution. Typically, beam instabilities have growth rates that are proportional to $n_e^{1/3}$[42], whereas the instability described here is not strongly dependent on density.

3. Simulations and laboratory experiment of maser emission

The idea that collisionless shock waves can accelerate electrons to high energy along the magnetic field direction has been demonstrated in a recent laboratory experiment using high energy lasers[22]. Modern high-power lasers are unique tools that are able to deliver pulses that have enormous energy densities to target. They allow measurements of plasma conditions that are of astrophysical interest, and allow testing the complex models of these processes with unprecedented precision. Laser-plasma results have been applied to the study of such diverse environments as active galactic nuclei and the Earth's bow shock. More recent applications include the hydrodynamics of supernovae, supernova remnants and the collision of galactic clouds[43, 44]. Such experiments are made possible by ensuring that certain key dimensionless parameters in the laser-generated plasmas have values similar to those of the space and astrophysical plasmas of interest. A recent paper in *Nature Physics*[22] reports on results from an experiment to investigate energetic particle production and X-ray emission from collisionless shock waves. In the experiment a 1 kJ, 1.5 ns laser beam of wavelength 527 nm impacted a 50 μm thick PVDF ($C_2H_2F_2$) foil target producing a high speed expanding plasma on the back surface with a velocity of 70 km/s. A 12-mm-diameter sphere was placed 15 mm from the foil, fabricated from either magnetized Nd with an approximately 7 kG surface field or unmagnetized glass. The fluorine ions within the expanding plasma have a kinetic energy of about 500 keV. When this plasma flow impacted the magnetized neodymium sphere, a strong collisionless bow shock formed ∼2.5 mm upstream of the object. Interferometric data showed that

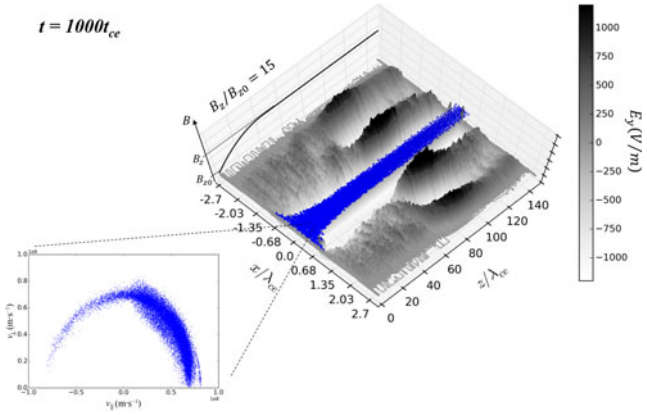

Figure 3. Composite overview of 3D VSim PIC simulation results in an x–z plane ($y = 0$) showing magnetic compression of an electron beam and subsequent cyclotron-maser emission in the X-mode at $t = 1000t_{ce}$. The electron PIC particle trajectory is also overlaid (blue scatter plot) along with the corresponding velocity distribution over the simulation volume at $t = 1000t_{ce}$.

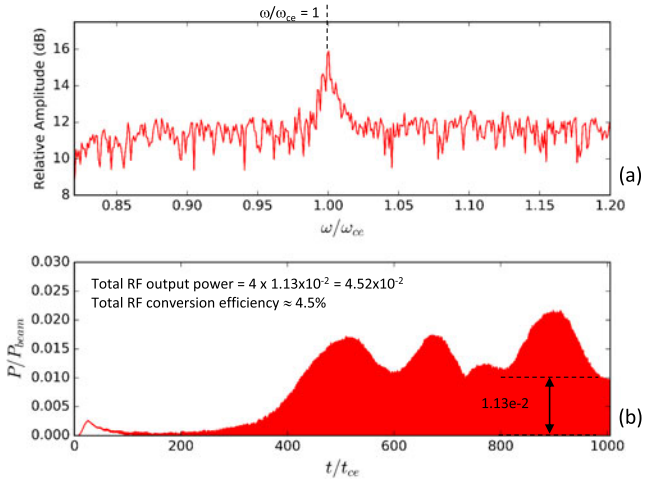

Figure 4. 3D VSim PIC simulation results showing (a) the spectrum of EM emission at $z = 86\lambda_{ce}$ and (b) the transverse Poynting flux in a y–z plane displaced from the electron beam.

the bulk electron density increased from $\sim 10^{17}$ cm^{-3} in the upstream region to $\sim 10^{18}$ cm^{-3} in the downstream region with a bulk plasma temperature of about 3 eV. An x–y spectrometer spatially resolved along the flow axis recorded soft X-rays in the range 630–770 eV including the fluorine line. This excess of X-rays is an indication that electrons with energies significantly greater than 3 eV must be present. No such results were observed with the un-magnetized sphere. To fully understand the interaction between the flowing plasma and a small magnetized object and assist in the experimental analysis, simulations were carried out using two numerical codes[22, 23]. A two-dimensional radiation-hydrodynamic code FLASH[22] was used together with a full PIC code OSIRIS[23]. The results from FLASH were in qualitative agreement with experiment, predicting the electric field influence on the plasma near the shock from the simulated magnetic field and ion density[22]. Experimental measurements inferred a super-critical shock with Mach number of $\sim$5.7, necessitating a significant reflected ion component. OSIRIS was able to determine the kinetics of the interaction demonstrating the formation of a shock, generation of an electric field resulting in reflection of ions, generation of lower hybrid waves and electron energization along the direction of the magnetic field[23]. These accelerated electrons, when moving into a stronger magnetic field, can evolve an unstable, pitch-spread velocity distribution having a horseshoe profile and capable of driving a cyclotron-maser instability that generates intense radio-frequency (RF) emission.

Laboratory experiments[37, 39] and PIC simulations[24, 38, 45] have demonstrated the high efficiency of the cyclotron-maser instability driven by electron horseshoe and ring-like velocity distributions. New numerical simulations have been carried out using the PIC code VSim[46], with the simulation geometry comprising a 3D Cartesian gridded region with axial length of $144\lambda_{ce}$ (where λ_{ce} is the vacuum wavelength of radiation at the peak electron-cyclotron frequency within the simulation), symmetric transverse dimensions of $2.7\lambda_{ce}$ and perfectly matched-layer boundaries in x, y and z to prevent reflection and the formation of boundary resonant eigenmodes. Particle absorbent boundaries are also used in x, y and z to terminate electron trajectories. An electron beam with energy 20 keV was injected parallel to an axial magnetic field that increased by a factor of 15 over $45\lambda_{ce}$, with the peak magnetic flux density of 0.1 T plateauing over the remaining $99\lambda_{ce}$, an electron number density n_e of $\sim 2.5 \times 10^{14}$ m^{-3} at the peak magnetic flux density and corresponding electron-cyclotron frequency to plasma frequency ratio of 20.

Figure 3 shows the transverse-electric field profile E_y as a surface plot in an x–z plane for 2% injected electron energy spread. The electron PIC particle trajectory is superimposed along with a projection of the axial magnetostatic field profile B_z in the left-vertical plane. The injected electrons are subject to significant magnetic compression, forming a horseshoe shaped velocity distribution upon entry to the peak-plateau region at $\sim 45\lambda_{ce}$ in z. From around $75\lambda_{ce}$ to $140\lambda_{ce}$ in z, there is clear evidence of cyclotron-maser emission in the X-mode, with wavefronts propagating near-perpendicularly to the axial magnetic field.

The corresponding wave spectrum is plotted in Figure 4(a), showing the fast Fourier transform (FFT) of E_y at $z = 86\lambda_{ce}$ over $t = 0 \rightarrow 1000t_{ce}$. A single spectral component is present at $\omega/\omega_{ce} = 1$, corresponding to narrowband emission at the relativistic electron-cyclotron frequency. The corresponding transverse Poynting flux over a y–z plane in Figure 4(b) demonstrates a temporal modulation of the wave emission, with a $350t_{ce}$ lead time for significant growth of the RF Poynting flux. A peak saturated output power of $P/P_{beam} = 1.13 \times 10^{-2}$ is observed. When integrated over the transverse dimensions of the system

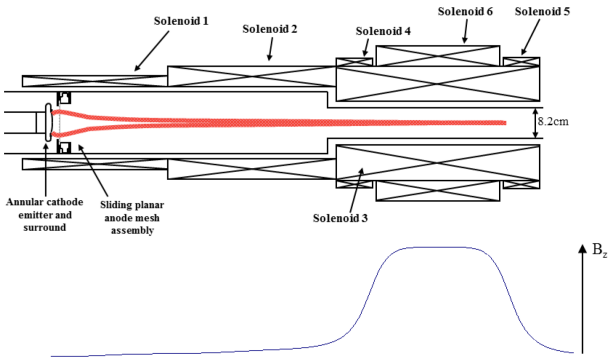

Figure 5. Diagrammatic overview of the experimental setup showing the magnetic coil configuration, electron gun and the convergent axial magnetic field profile with peak-plateau region for cyclotron resonant energy transfer.

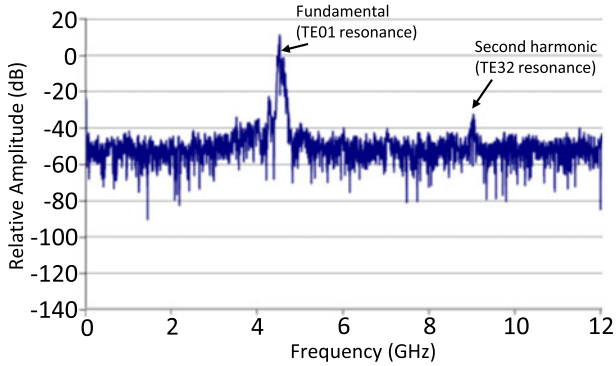

Figure 6. Experimental measurements for the TE01 resonance, illustrating the spectrum of the output signal, displaying a strong resonance close to the electron-cyclotron frequency, 4.42 GHz.

(factoring in the 4 enclosing Poynting flux planes) this corresponds to an RF conversion efficiency of 4.50% which is in agreement with estimates from theory and consistent with estimates for the auroral kilometric radiation (AKR) generation efficiency[7].

A scaled laboratory experiment conducted at the University of Strathclyde, Glasgow, UK demonstrated the principles of electron beam magnetic compression/horseshoe formation and cyclotron-maser emission at microwave frequencies[24, 37–39]. A schematic overview of the experiment is presented in Figure 5, showing the annular electron beam injected into a convergent magnetic field (with magnetic mirror ratios ranging from 15 to 30). The beam traversed into a circular-cylindrical waveguide post-compression, where excitation of X-mode like transverse-electric (TE) modes near cutoff ($k_{\|} \approx 0$) occurred via the cyclotron-maser instability. Figure 6 shows the spectral output for a peak magnetic flux density of 0.18 T. A primary spectral peak is present at the electron-cyclotron frequency (4.42 GHz) and a small second harmonic peak at around 8.8 GHz. The corresponding output power for this experiment was 30 kW, equating to a beam-wave conversion efficiency of 1%[39]. Both the spectral output and beam-wave conversion efficiencies are consistent with the predictions of theory[36] and PIC simulations[24, 38].

4. Summary and conclusions

In this article, we have described an acceleration scheme by which electrons may be energized at collisionless shocks. Propagation of these electrons into stronger magnetic field regions results in the formation of a horseshoe or thermal-ring-like distribution in velocity space. We outline a model by which such distributions can become unstable to a cyclotron-maser instability resulting in intense, narrowband radio emission in the X-mode with an efficiency of a few percent. In particular, the combination of lower-hybrid acceleration within collisionless shocks, diffusion of energetic electrons into increasing magnetic fields and the subsequent cyclotron-maser destabilization of the resultant electron velocity distributions provides an excellent framework for explaining radio emission from astrophysical jets, consistent with the suggestions of Begelman, Ergun and Rees[3]. We report on recent laboratory experiments[37–39] where energetic electrons with horseshoe-type distribution functions are unstable to the generation of maser radiation. Through theory, numerical simulations[23, 24, 45, 47] and laboratory experiments, the sub-elements and principal physics of this model have been explored. The results are relevant to a variety of astrophysical plasma environments including blazar jets[3, 4, 19, 20, 47].

Acknowledgements

The research leading to the results in this article has received funding from the Engineering and Physical Sciences Research Council (grant Nos. EP/N014472/1, EP/R004773/1 and EP/N013298/1) and the Science and Technologies Facilities Council of the United Kingdom. F.C. and L.O.S. acknowledge support from the European Research Council (InPairs ERC-2015-AdG 695088) and FCT Portugal (grant No. PD/BD/114307/2016). This work was supported in part at the University of Chicago by the US DOE NNSA ASC through the Argonne Institute for Computing in Science under FWP 57789 and the US DOE Office of Science through grant No. DE- SC0016566.

References

1. D. L. Meier, S. Koide, and Y. Uchida, Science **291**, 84 (2001).
2. R. S. Nemmen, M. Georganopoulos, S. Guiriec, E. T. Meyer, N. Gehrels, and R. M. Sambruna, Science **338**, 1445 (2012).
3. M. C. Begelman, R. E. Ergun, and M. J. Rees, Astrophys. J. **625**, 51 (2005).
4. R. Bingham, B. J. Kellett, R. A. Cairns, J. Tonge, and J. T. Mendonca, Astrophys. J. **595**, 279 (2003).
5. R. A. Treumann, Astron. Astrophys. Rev. **13**, 229 (2006).
6. S. P. O'Sullivan and D. C. Gabuzda, Mon. Not. R. Astron. Soc. **400**, 26 (2009).

7. D. A. Gurnett, J. Geophys. Res. **79**, 4227 (1974).
8. T. Katsouleas and J. M. Dawson, Phys. Rev. Lett. **51**, 392 (1983).
9. J. B. McBride, E. Ott, J. P. Boris, and J. H. Orens, Phys. Fluids **15**, 2367 (1972).
10. M. Yamada and D. K. Owens, Phys. Rev. Lett. **38**, 1529 (1977).
11. K. G. McClements, R. Bingham, J. J. Su, J. M. Dawson, and D. S. Spicer, Astrophys. J. **409**, 465 (1993).
12. M. J. Laming, Astrophys. J. **563**, 828 (2001).
13. J. Vink and M. J. Laming, Astrophys. J. **584**, 758 (2003).
14. V. D. Shapiro and V. I. Shevchenko, Sov. Sci. Rev. E **6**, 425 (1988).
15. R. Bingham, J. M. Dawson, V. D. Shapiro, D. A. Mendis, and B. J. Kellett, Science **275**, 49 (1997).
16. R. Bingham, B. J. Kellett, J. M. Dawson, V. D. Shapiro, and D. A. Mendis, Astrophys. J. **127**, 233 (2000).
17. R. Bingham, B. J. Kellett, P. Bryans, H. P. Summers, M. Torney, V. D. Shapiro, D. S. Spicer, and M. O'Brien, Astrophys. J. **601**, 896 (2004).
18. R. Bingham, V. D. Shapiro, V. N. Tsytovich, U. de Angelis, M. Gilman, and V. I. Shevchenko, Phys. Fluids B **3**, 1728 (1991).
19. R. A. Bamford, B. Kellett, W. J. Bradford, C. Norberg, A. Thornton, K. J. Gibson, I. A. Crawford, L. Silva, L. Gargat é, and R. Bingham, Phys. Rev. Lett. **109**, 081101 (2012).
20. R. A. Bamford, E. P. Alves, F. Cruz, B. J. Kellett, R. A. Fonseca, L. O Silva, R. M. G. M. Trines, J. S. Halekas, G. Kramer, and E. Harnett, Astrophys. J. **830**, 146 (2016).
21. R. Bingham, R. Bamford, B. J. Kellett, and V. D. Shapiro, J. Plasma Phys. **76**, 915 (2010).
22. A. Rigby, F. Cruz, B. Albertazzi, R. Bamford, A. R. Bell, J. E. Cross, F. Fraschetti, P. Graham, Y. Hara, P. M. Kozlowski, Y. Kuramitsu, D. Q. Lamb, S. Lebedev, J. R. Marques, F. Miniati, T. Morita, M. Oliver, B. Reville, Y. Sakawa, S. Sarkar, C. Spindloe, R. Trines, P. Tzeferacos, L. O. Silva, R. Bingham, M. Koenig, and G. Gregori, Nat. Phys. **14**, 475 (2018).
23. F. Cruz, E. P. Alves, R. A. Bamford, R. Bingham, R. A. Fonseca, and L. O. Silva, Phys. Plasmas **24**, 022901 (2017).
24. D. C. Speirs, R. Bingham, R. A. Cairns, I. Vorgul, B. J. Kellett, A. D. R. Phelps, and K. Ronald, Phys. Rev. Lett. **113**, 155002 (2014).
25. P. Drake, *High-Energy-Density Physics: Foundation of Inertial Fusion and Experimental Astrophysics* (Springer International Publishing, 2006).
26. B. A. Remington, R. P. Drake, and D. D. Ryutov, Rev. Mod Phys. **78**, 755 (2006).
27. M. E. Koepke, Rev. Geophys. **46**, RG3001 (2008).
28. S. Lebedev, L. Suttle, G. F. Swadling, M. Bennett, S. N. Bland, G. C. Burdiak, D. Burgess, J. P. Chittenden, A. Ciardi, A. Clemens, P. de Grouchy, G. N. Hall, J. D. Hare, N. Kalmoni, N. Niasse, S. Patankar, L. Sheng, R. A. Smith, F. Suzuki-Vidal, J. Yuan, A. Frank, E. G. Blackman, and R. P. Drake, Phys. Plasmas **21**, 056305 (2014).
29. G. Gregori, B. Reville, and F. Miniati, Phys. Rep. **601**, 1 (2015).
30. D. D. Ryutov, B. A. Remington, H. F. Robey, and R. P. Drake, Phys. Plasmas **8**, 1804 (2001).
31. R. Cesario, L. Amicucci, C. Castaldo, M. Kempenaars, S. Jachmich, J. Mailloux, O. Tudisco, A. Galli, and A. Krivska, and JET-EFDA contributors, Plasma Phys. Control. Fusion **53**, 085011 (2011).
32. V. D. Shapiro, R. Bingham, J. M. Dawson, Z. Dobe, B. J. Kellett, and D. A. Mendis, J. Geophys. Res. **104**, 2537 (1999).
33. Y. Omelchenko, A. Yu. R. Z. Sagdeev, V. D. Shapiro, and V. I. Shevchenko, Sov. J. Plasma Phys. **15**, 739 (1989).
34. J. A. Eilek and J. C. Weatherall, in *Diffuse Thermal and Relativistic Plasma in Galaxy Clusters*, H. Bohringer, L. Feretti and P. Schuecker (eds) (Max-Planck-Institut für Extraterrestrische Physik, Garching, Germany, 1999), p. 249.
35. J. A. Eilek, Phys. Plasmas **10**, 1539 (2003).
36. R. Bingham and R. A. Cairns, Phys. Plasmas **7**, 3089 (2000).
37. K. Ronald, D. C. Speirs, S. L. McConville, A. D. R. Phelps, C. W. Robertson, C. G. Whyte, W. He, K. M. Gillespie, A. W. Cross, and R. Bingham, Phys. Plasmas **15**, 056503 (2008).
38. D. C. Speirs, S. L. McConville, K. M. Gillespie, K. Ronald, A. D. R. Phelps, A. W. Cross, R. Bingham, C. W. Robertson, C. G. Whyte, and I. Vorgul, Plasma Phys. Control. Fusion **50**, 074011 (2008).
39. S. L. McConville, D. C. Speirs, K. Ronald, A. D. R. Phelps, A. W. Cross, R. Bingham, C. W. Robertson, C. G. Whyte, W. He, K. M. Gillespie, I. Vorgul, R. A. Cairns, and B. J. Kellett, Plasma Phys. Control. Fusion **50**, 074010 (2008).
40. D. B. Melrose, Rev. Mod. Plasma Phys. **1**, 5 (2017).
41. T. H. Stix, *Waves in Plasma* (AIP, New York, 1992).
42. N. Krall and A. W. Trivelpiece, *Principles of Plasma Physics* (McGraw Hill, New York, 1973).
43. A. Scopatz, M. Fatenejad, N. Flocke, G. Gregori, M. Koenig, D. Q. Lamb, D. Lee, J. Meinecke, A. Ravasio, P. Tzeferacos, K. Weide, and R. Yurchak, High Energy Density Phys. **9**, 75 (2013).
44. J. Meinecke, H. W. Doyle, F. Miniati, A. R. Bell, R. Bingham, R. Crowston, R. P. Drake, M. Fatenejad, M. Koenig, Y. Kuramitsu, C. C. Kuranz, D. Q. Lamb, D. Lee, M. J. MacDonald, C. D. Murphy, H.-S. Park, A. Pelka, A. Ravasio, Y. Sakawa, A. A. Schekochihin, A. Scopatz, P. Tzeferacos, W. C. Wan, N. C. Woolsey, R. Yurchak, B. Reville, and G. Gregori, Nat. Phys. **10**, 520 (2014).
45. D. C. Speirs, K. Ronald, S. L. McConville, K. M. Gillespie, A. D. R. Phelps, A. W. Cross, R. Bingham, C. W. Robertson, C. G. Whyte, W. He, I. Vorgul, R. A. Cairns, and B. J. Kellett, Phys. Plasmas **17**, 056501 (2010).
46. C. Nieter and J. R. Cary, J. Comput. Phys. **196**, 448 (2004).
47. R. Bingham, D. C. Speirs, B. J. Kellett, I. Vorgul, S. L. McConville, R. A. Cairns, A. W. Cross, A. D. R. Phelps, and K. Ronald, Space Sci. Rev. **178**, 695 (2013).